

I.F. Mironyuk<sup>1</sup>, T.R. Tatarchuk<sup>2</sup>, H.V. Vasylyeva<sup>3</sup>, I.P. Yaremiy<sup>4</sup>, I.M. Mykytyn<sup>1</sup>

## Morphology, Phase Composition and Radiological Properties of Fly Ash Obtained from the Burshtyn Thermal Power Plant

<sup>1</sup>*Department of Chemistry, Faculty of Natural Science, Vasyl Stefanyk Precarpathian National University, Ivano-Frankivsk, 76018, Ukraine*

<sup>2</sup>*Educational and Scientific Center of Material Science and Nanotechnology, Vasyl Stefanyk Precarpathian National University, Ivano-Frankivsk, 76018, Ukraine*

<sup>3</sup>*Department of Physics of Nucleus and Elementary Particles, Department of Theoretical Physics, Uzhgorod National University, Uzhgorod, 88000, Ukraine*

<sup>4</sup>*Department of Materials Science and New Technologies, Vasyl Stefanyk Precarpathian National University, Ivano-Frankivsk, 76018, Ukraine*

The physico-chemical properties of ash extracted from smoke during the combustion of coal at the Burshtyn thermal power plant were investigated. The particles formed in the flame are crystallized glass beads with a size of 0.8–600 μm. It was found that the ash particles are heterogeneous in their chemical composition. The mass content of the ferric oxides can vary from 2.1 % to 96.4 %, however, despite this, the Al<sub>2</sub>O<sub>3</sub>/SiO<sub>2</sub> ratio in the glass balls remains constant at a value of 0.47 ± 0.02. Phase analysis confirmed the presence of α-quartz particles (~ 62 wt%), mullite (~ 32 wt%) and α-FeOOH, α-Fe<sub>2</sub>O<sub>3</sub> and Fe<sub>3</sub>O<sub>4</sub> mixtures (totaling 6 wt%). Radiological studies have revealed higher β- and γ-activity of fly ash, selected from the dump, compared with the fly ash from the electro-filter. This is due to the accumulation of <sup>214</sup>Pb and <sup>214</sup>Bi radionuclides particles formed on the surface of the particles due to decay of <sup>222</sup>Rn.

**Key words:** fly ash, glass microspheres, mullite, quartz, radiology.

*Article acted received 02.04.2018; accepted for publication 15.06.2018.*

### Introduction

During the combustion of coal, anthracite or combustible shale on the thermal power plants (TPPs), the solid wastes are produced in the form of slag (with the particle size <1 mm) and fine fly ash. The amount of this waste relative to burned coal can be up to 16 % [1]. Slag wastes are used as components of concrete mixtures, as basis for building slag blocks, etc. However, fly ash presents a difference from slag both in particles morphology and in phase composition therefore, it is not widely used. Fly ash small particles generated in the coal combustion zone, are driven by flue gas, caught by an electrofilter, mixed with water in the form of a suspension, and then transported to an ash dump. In Ukraine, about 8 million tons of waste is accumulated annually, but only 5% is being used. About 400 million tons of fly ash is concentrated in the Ukrainian TPP dumps. About 40 million tons of fly ash accumulate in the bins of Burshtyn TPP [2, 3]. Such wastes are the reason of environmental pollution. Fly ash is spread by the wind and causes air contamination, changes the

chemical and mineralogical composition of the soil. Impregnation of water from ash dumps to the ground leads to the dissipation of pollutants (heavy metals, radionuclides) into underground waters, and with them – in rivers, from where people are using water.

According to the literary data, the state of utilization of the fly ashes by TPPs is satisfactory in Finland, Great Britain and Germany [4-6]. In the European Union, 50% of the fly ashes are processed into useful products, and in the US - only 25%. In many countries, research is being carried out on the creation of new technologies, for example, for the production of cement, concrete products, as well as during construction of roads [5, 7]. Undoubtedly, the in-depth study of the physico-chemical properties of the fly ash of each TPP will accelerate the search for new enrichment or modification technologies that will ultimately expand the applications of these mineral waste.

The aim of this paper is to investigate the morphology, phase composition and radiological properties of fly ash from the Burshtyn TPP.

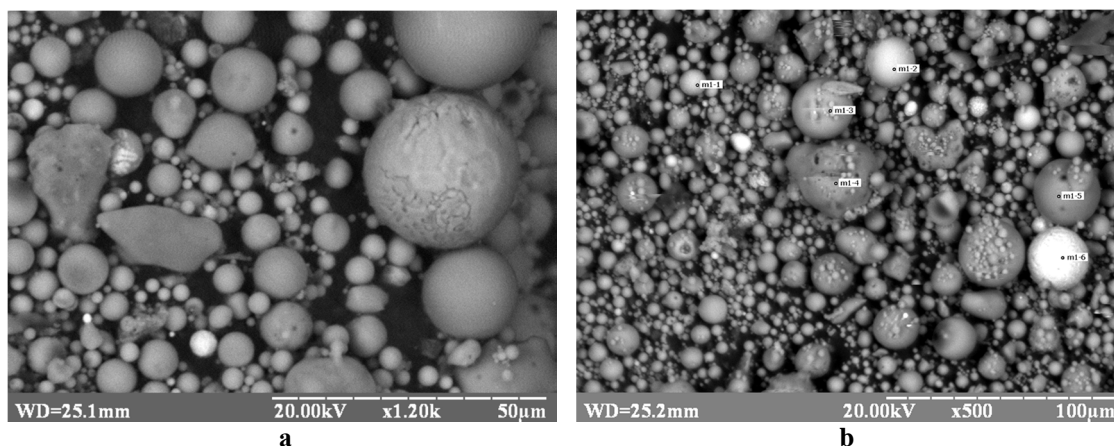


**Fig. 1.** SEM of fly ash particles: a – magnification  $\times 1200$  times; b - magnification  $\times 500$  times (the elemental composition was determined in the balls marked with the labels in the image b).

## I. Materials and Methods

The samples of fly ash were selected in two places: the first place is from an electrofilter, in which the ash is removed from the chimney gases, and the second place is from ash-store, where it is stored.

The morphology of the fly ash particles was investigated using a scanning electron microscope REMMA-102-02 (Ukraine), coupled with an express-analyzer of the elemental composition of the samples. X-ray fluorescence analyzer EXPERT-3L (Ukraine) was used for the precise determination of the elemental composition of the samples.

The size distribution of the fly ash particles, as well as their specific surface area, was investigated by the Malvern Mastersizer 3000 E laser diffraction particle size analyzer (England). Ethanol was used as a dispersion medium.

The phase composition of fly ash was determined by X-ray diffractometer DRON-3.0 equipped with Cu-K $\alpha$  radiation. XRD patterns were analyzed by the Rietveld method using the software FullProf.

The structure of the fly ash particles was investigated by infrared spectroscopy (IR spectroscopy). The sample (4 mg) was mixed with KBr in a 1: 100 ratio and homogenized in a vibrating mill for 5 minutes. The prepared mixture was compressed by forming a plate of 8  $\times$  20 mm and mass 20 mg. The spectra were recorded on the spectrophotometer SPECORD M80 (Germany).

For radiological studied of fly ash, a dosimeter, G-M detector and gamma spectrometer were used. The average dose in Roentgen per second ( $\mu\text{P}\cdot\text{s}^{-1}$ ) of radiation was measured by dosimeter “SRP-6801”. The  $\beta$ -activity of fly ash was measured using G-M detector with applied voltage 400 V. The gamma spectra were obtained using scintillated detector with NaI(Tl), equipped with program AkWin. We calibrated gamma spectrometer with standard gamma sources  $^{137}\text{Cs}$  and  $^{60}\text{Co}$ . The gamma spectrometer efficiency ( $\varphi$ ) was 9 %. Applied voltage – 1100 V. Instruments manufactured by the enterprise “Atom Complex device” (Ukraine). The

average activity was measured using equation:  $A = N_{\text{imp}} - N_b / m \cdot t \cdot \varphi \cdot I_\gamma$ , where  $N_{\text{imp}}$  – number of pulses in characteristic peaks from samples of fly ash;  $N_b$  – number of pulses from background radiation;  $I_\gamma$  – yield of gamma line of the isotope;  $\varphi$  – spectrometer efficiency (%);  $t$  – measured time (s);  $m$  – mass of the sample (kg).

## II. Experimental results and discussion

The shape of the particles and the phase state of the fly ash depend both on the mineral composition of coal and the temperature of its combustion. If the total content of oxides SiO $_2$ , Al $_2$ O $_3$ , Fe $_2$ O $_3$  in ash more than 70%, the fly ash is called acidic. If the amount of these oxides is in the range 50-70 %, then such fly ash is called basic. The particles of fly ash are usually micro-spherical, and the particles of the basic ash have irregular shape [8, 9].

SEM images of the fly ash particles are shown in Fig. 1 and they confirm that particles have a micro-spherical shape. The particle size distributions is shown in Fig. 2. The specific surface area and the di

The smallest particles in the fly ash have a size of 0.8  $\mu\text{m}$ , and the largest ones are 600  $\mu\text{m}$ . The maximum peak on the integral curve corresponds to particles having a size of  $\sim 16 \mu\text{m}$ . The volume fraction of these particles is the largest – 4.5 %. In the fly ash, the fraction with size

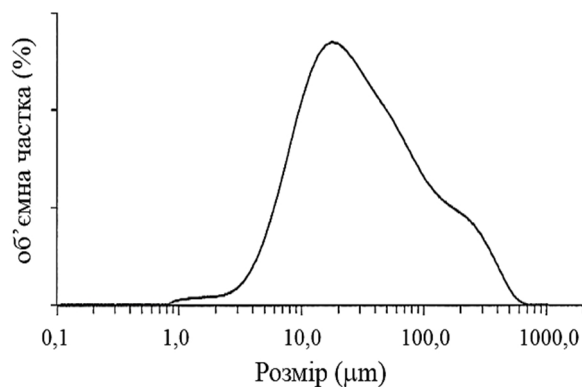


**Fig. 2.** The particle size distributions of fly ash.

**Table 1**

The specific surface area and size distributions of fly ash

Specific surface area, $\text{cm}^2 \cdot \text{g}^{-1}$	Fraction particle size ( $\mu\text{m}$ ) and volume fraction (%)			
	0,8-32	32-63	63-200	200-600
171	54,8	18,3	19,3	7,6

**Table 2**

Chemical composition of fly ash

Oxide component	The mass content of the components, %	
	Fly ash from the electrofilter	Fly ash from the dump
SiO <sub>2</sub>	56,373 ± 0,067	56,708 ± 0,063
Al <sub>2</sub> O <sub>3</sub>	21,177 ± 0,071	22,623 ± 0,070
Fe <sub>2</sub> O <sub>3</sub>	9,390 ± 0,018	9,344 ± 0,016
K <sub>2</sub> O	4,367 ± 0,065	4,504 ± 0,063
CaO	3,675 ± 0,037	2,525 ± 0,031
MgO	1,500 ± 0,088	1,861 ± 0,082
TiO <sub>2</sub>	1,121 ± 0,012	1,149 ± 0,011
Na <sub>2</sub> O	0,826 ± 0,008	0,471 ± 0,008
P <sub>2</sub> O <sub>5</sub>	0,214 ± 0,007	0,248 ± 0,006
SO <sub>3</sub>	0,980 ± 0,005	0,209 ± 0,003
MnO <sub>2</sub>	0,076 ± 0,0002	0,078 ± 0,0002
V <sub>2</sub> O <sub>5</sub>	(448 ± 50) · 10 <sup>-6</sup>	(489 ± 49) · 10 <sup>-6</sup>
SrO	(472 ± 5) · 10 <sup>-6</sup>	(441 ± 4) · 10 <sup>-6</sup>
ZrO <sub>2</sub>	(358 ± 5) · 10 <sup>-6</sup>	(335 ± 4) · 10 <sup>-6</sup>
Ni <sub>2</sub> O <sub>3</sub>	(242 ± 7) · 10 <sup>-6</sup>	(228 ± 6) · 10 <sup>-6</sup>
Cr <sub>2</sub> O <sub>3</sub>	(162 ± 21) · 10 <sup>-6</sup>	(199 ± 21) · 10 <sup>-6</sup>

The total content of Rb<sub>2</sub>O, CuO, Y<sub>2</sub>O<sub>3</sub>, GeO<sub>2</sub>, Ag<sub>2</sub>O i Nb<sub>2</sub>O<sub>5</sub> oxides in the fly ash from the dump is 7 · 10<sup>-4</sup> %, and in the fly ash from the electrofilter – 7,5 · 10<sup>-4</sup> %.

of 0.8 - 32  $\mu\text{m}$  is dominant and represents about 54.8 % (Table 1).

Elemental composition of fly ash, determined by X-ray fluorescence analysis, was recalculated in the mass content of their oxides. Table 2 shows the chemical composition of particles taken from the electrofilters and the dump.

Data analysis shows that fly ash from the dump, due to its contact with the sediments, the content of Na<sub>2</sub>O and CaO decreases in comparison with the fly ash taken from the electrofilter, from 0.86 to 0.47 % and from 3.675 to 2.525 %, respectively. The SO<sub>3</sub> content is also reduced from 0.980 to 0.209 % in the fly ash. The changes in their chemical composition are due to the washing out of water-soluble compounds (Na<sub>2</sub>SO<sub>4</sub>) from the surface

**Table 3**

Chemical composition of fly ash microspheres

Component of fly ash	Oxide compounds in the microspheres, wt. %					
	M1-1	M2-2	M1-3	M1-4	M1-5	M1-6
Na <sub>2</sub> O	0,62	0,33	1,0	1,20	1,34	0,02
MgO	2,54	1,76	2,63	2,07	0,63	0,09
Al <sub>2</sub> O <sub>3</sub>	19,72	13,35	26,2	26,18	28,70	0,93
SiO <sub>2</sub>	42,82	28,35	53,15	57,5	61,02	2,01
K <sub>2</sub> O	2,3	2,00	3,52	4,39	3,99	0,01
CaO	1,02	2,37	1,3	0,71	0,12	0,24
TiO <sub>2</sub>	0,77	1,06	0,77	0,58	0,09	0,27
Fe <sub>x</sub> O <sub>y</sub>	30,21	50,18	11,43	6,00	2,10	96,43

layer. In turn, at pH < 7, Ca<sup>2+</sup> cations are replaced by protons of H<sup>+</sup>.

The EDS analysis allows to trace the changes in the chemical composition in the fly ash micro-spheres. Depicted in Fig. 1 ash particles, in which the chemical content of the components was determined, are indicated by the corresponding numbers M1-1, M2-2, M1-3, M1-4, M1-5, M1-6. The results of the studies presented in Table 3 show a significant difference in their chemical composition.

In particular, in the six spheres labeled M1-1, M2-2, M1-3, M1-4, M1-5, and M1-6, the mass content of ferric oxides varies considerably from 2.1 to 96.43%. It is important to highlight how the ratio between Al<sub>2</sub>O<sub>3</sub>, CaO, Na<sub>2</sub>O, K<sub>2</sub>O, MgO, TiO<sub>2</sub> and silica increases as Fe<sub>x</sub>O<sub>y</sub> increases. From Fig. 3, it can be seen that despite the change in the chemical composition, the ratio of Al<sub>2</sub>O<sub>3</sub>/SiO<sub>2</sub> in the spheres remains constant at a value of 0.47 ± 0.02. The K<sub>2</sub>O/SiO<sub>2</sub> ratio, which is approximately 0.066, is also constant. With the increase of ferric oxides content, the values CaO/SiO<sub>2</sub> and MgO/SiO<sub>2</sub> ratios increase from 0.002 to 0.12 and from 0.01 to 0.044 (Fig. 3, curves 2 and 3) respectively. In these conditions, the TiO<sub>2</sub>/SiO<sub>2</sub> ratio also increases from 0.002 to 0.143 (Fig.3, curve 4), and the value of Na<sub>2</sub>O/SiO<sub>2</sub> decreases from 0.022 to 0.009 (curve 5).

Consequently, the obtained results of the dispersion and the chemical composition of the fly ash are evidenced by its heterogeneity in both particle size and content of the components.

The X-ray diffraction pattern of the of fly ash as depicted in Fig. 4 indicates the presence of few microcrystalline phases in its composition. A detailed analysis of the diffraction pattern reveal that the main phases in the fly ash particles are  $\alpha$ -quartz (~ 62 wt%), mullite Al<sub>2.4</sub>Si<sub>0.6</sub>O<sub>4.8</sub> (~ 32 wt%), and a mixture of ferrous compounds – goethite  $\alpha$ -FeOOH, hematite  $\alpha$ -Fe<sub>2</sub>O<sub>3</sub> and magnetite Fe<sub>3</sub>O<sub>4</sub> (total 6% by weight). Structural characteristics of the identified phases are given in Table 4.

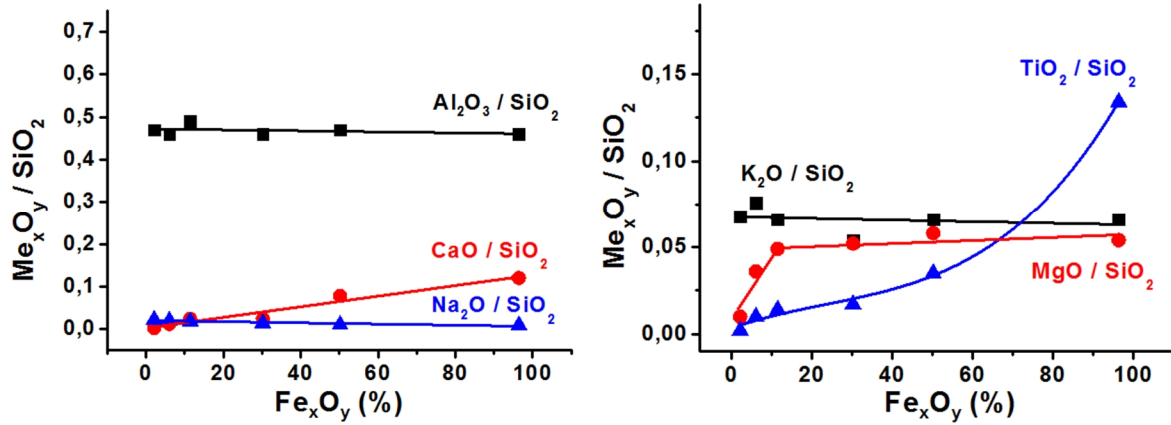


Fig. 3. Changes in the ratio between oxide components and silica in the fly ash particles with iron oxides ( $Fe_xO_y$ ) increasing.

Table 4

Structural characteristics of crystalline phases of fly ash.

Structural characteristics	Phases				
	SiO <sub>2</sub> (quartz)	Al <sub>2,4</sub> Si <sub>0,6</sub> O <sub>4,8</sub> (mullite)	α-FeO(OH) (goethite)	Fe <sub>3</sub> O <sub>4</sub> (magnetite)	
Space group symmetry	P 32/21	Pbam (55)	Pbnm (62)	Fd3m (227)	
Lattice parameter, nm	a	0,4919 ± 3 · 10 <sup>-4</sup>	0,75880 ± 5 · 10 <sup>-4</sup>	0,4625 ± 6 · 10 <sup>-4</sup>	0,8396 ± 6 · 10 <sup>-4</sup>
	b	0,4919 ± 3 · 10 <sup>-4</sup>	0,75880 ± 5 · 10 <sup>-4</sup>	0,9990 ± 6 · 10 <sup>-4</sup>	–
	c	0,5413 ± 5 · 10 <sup>-4</sup>	0,28895 ± 6 · 10 <sup>-4</sup>	0,3037 ± 7 · 10 <sup>-4</sup>	–

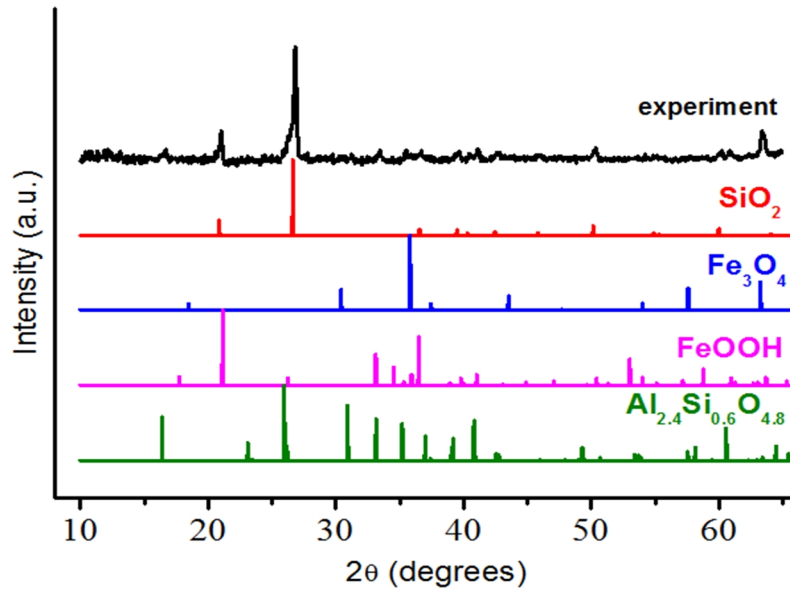


Fig. 4. The diffraction pattern of the fly ash (experiment) and the bar graph of its microcrystalline phases.

The elemental composition of the mullite corresponds to the chemical formula  $Al_6Si_2O_{13}$  ( $3Al_2O_3 \cdot 2SiO_2$ ). The mullite phase of  $Al_{2,4}Si_{0,6}O_{4,8}$  ( $2Al_2O_3 \cdot SiO_2$ ) in fly ash micro-spheres is a non-stoichiometric compound that contains an excess of Al atoms. This is due to the fact that mullite forms solid solutions with  $Al_2O_3$  [10].

To determine the structural characteristics of the Fe-containing fly ash micro-crystals, the magnetic particles were removed from the powder material by an external magnet. The magnetic fly ash fraction contains 29% α-

quartz, 50%  $Fe_3O_4$  and 21% α- $Fe_2O_3$ . Comparing the parameters of the micro-crystalline phases encapsulated in the vitreous matrix of fly ash particles, with the parameters of the corresponding crystalline phases, which are contained in the literature, some differences in their values are noticed. The cell parameters of α-quartz micro-crystals given in Table 4 are larger than that of ordinary crystals α-quartz [11] ( $a = b = 0.41414$  nm;  $c = 0.54060$  nm). The lattice parameter of  $Fe_3O_4$  micro-crystals in the fly ash particles is close to the lattice parameter of this phase as an independent material ( $a =$

0.8396 nm) [12]. In this case, the effect of pressure is insignificant, since the micro-crystals are relatively large.

The increase in the lattice parameters of  $\alpha$ -quartz and mullite micro-crystals indicates the presence of large mechanical stresses inside the fly ash micro-spherical particles. The tensile state of the micro-crystalline phases is due to the effect of considerable pressure from the vitreous matrix side. It is related to the crystallization of glass spheres at high temperatures.

Consider the sequence of fly ash formation processes in a flame. The aerosol particles  $\text{SiO}_2$ ,  $\text{AlOOH}$ ,  $\alpha$ - $\text{FeOOH}$ ,  $\text{MgCO}_3$ ,  $\text{CaCO}_3$ ,  $\text{Na}_2\text{O}$ ,  $\text{K}_2\text{O}$  or a mixture of these compounds, formed during the coal combustion at temperatures of 1000 -1500°C, are driven by gaseous products and hot air from the fire zone. Under the action of turbulent diffusion, small particles are assembled into aggregates and associates. The melting components in the associates contribute to the formation of melted drops, which become glass spheres during cooling. It should be noted that the associates formed from silica and aluminosilicate components instantly melt at a temperature of 900-1100°C, while the associatives containing silica and Fe-containing compounds are molting at a temperature  $\geq 1100^\circ\text{C}$ . Thus, the heterogeneity of temperature in the coal combustion zone and, consequently, the different degree of turbulence of waste gases lead to the formation of different size fly ash and heterogeneous chemical composition. The crystallization of glass spheres begins in a molten state and continues at high temperatures and in solid state. An increase in the size of a micro-droplet of glass is limited only by the temperature of the flame and the time they are in it.

The formation of mullite and magnetite inside the glass spheres is accompanied by an increase in their specific volume. According to the literature data, the density of the mullite is  $3.16 \text{ g}\cdot\text{cm}^{-3}$  and it is smaller than the density of  $\alpha$ - $\text{Al}_2\text{O}_3$  ( $3.96 \text{ g}\cdot\text{cm}^{-3}$ ), and the density of magnetite is  $5.18 \text{ g}\cdot\text{cm}^{-3}$  and also less than the density of output phases of  $\text{FeO}$  ( $5.7 \text{ g}\cdot\text{cm}^{-3}$ ) and  $\alpha$ - $\text{Fe}_2\text{O}_3$  ( $5.25 \text{ g}\cdot\text{cm}^{-3}$ ) [13]. The increase in the specific volume of crystallites causes strain in glass spheres. Significant pressure from the side of the vitreous matrix leads to a decrease in the valence angle Si-O-Si, Al-O-Al, Fe-O-Fe, which bond octahedrons or tetrahedrons in the lattice. Due to this convergence of the cations in the sublattices and due to the emergence of repulsive electrostatic force between them is compensated by elongation of bonds. This effect results in an increase in the parameters of the micro-crystal phases.

Mechanical strains in the volume of crystallized fly ash particles cause to the growth of their hardness. In particular, through the micro-crystallization of special grades of glass the high-strength materials - sitals could be obtained [14].

The FTIR spectrum of the fly ash, as depicted in Fig. 5, contains an intense broad band with a maximum intensity at  $1064 \text{ cm}^{-1}$ , which belongs to asymmetric oscillations of siloxane bridges Si-O-Si in quartz crystallites [11]. The contour of this band also covers individual strips due to asymmetric oscillations of atoms from Si-O-Al, Al-O-Al bonds. The symmetric valence

oscillation of siloxane bridges corresponds to a band of  $810 \text{ cm}^{-1}$  [15].

Deformation vibrations of  $\text{SiO}_4$  tetrahedrons in micro-crystallites and vitreous matrix are indicated by the band located at  $452 \text{ cm}^{-1}$ . Such fluctuations are recorded in the range of  $450 - 500 \text{ cm}^{-1}$  for other  $\text{SiO}_2$  modifications (coesite, quartz, cristobalite, tridymite) [11].

The bands with weak intensity observed at 1356, 880,  $796 \text{ cm}^{-1}$  are characteristic for  $\alpha$ - $\text{FeOOH}$  and the vibration of Fe-O bonds within the goethite structure [16]. The bands at 612 and  $424 \text{ cm}^{-1}$ , manifest the variations of the  $\text{Fe}_3\text{O}_4$  lattice.

Separate weak intensity bands in the fly ash spectrum indicate the presence in the volume of its inclusions particles of carbon clusters. In particular, the bands at 570, 1508 and  $1640 \text{ cm}^{-1}$  are characteristic vibrations of atoms in a hexagonal graphene cycles [17].

Radiation that originates on Earth is called terrestrial radiation. Radionuclides that were present when the Earth formed are referred to as primordial. The coal extracted from the Earth's crust can contain primordial radionuclides, include the series of radionuclides produced when Uranium and Thorium decay, as well as Potassium-40 (half-life  $1.39 \cdot 10^9$  year) and Rubidium-87 (half-life  $4.88 \cdot 10^{10}$  year) [18, 19].

During coal combustion, radionuclides are absorbed by molten particles of fly ash. As a result, the content of (for example) Uranium in fly ash exceeds its content in some types of coal in 2,5-6 times [3].

The radioactivity of materials is estimated by their specific activity  $A_s$  ( $\text{Bq}\cdot\text{kg}^{-1}$ ) [23]:

$$A_s = A_{\text{Ra}} + 1,31 A_{\text{Th}} + 0,085 A_{\text{K}}, \quad (2)$$

where  $A_{\text{Ra}}$ ,  $A_{\text{Th}}$ ,  $A_{\text{K}}$  – specific activity of Radium, Thorium and Potassium in the sample.

Dose (Radiation Dose) refers to the effect on a material that is exposed to radiation. It can denote the amount of energy absorbed by a material. In this work, the dose of background radiation was calculated as the arithmetic mean of 26 measurements and it is equal  $0,0719 \pm 0,0058 \mu\text{P}\cdot\text{s}^{-1}$ . The radiation doses from fly ash from an electro-filter and fly ash from the dump are equal to  $0,0708 \pm 0,0056 \mu\text{P}\cdot\text{s}^{-1}$  i  $0,0731 \pm 0,0063 \mu\text{P}\cdot\text{s}^{-1}$  respectively. Therefore, the average dose of gamma radiation of the studied samples is at the background level.

The average  $\beta$ -activity of samples is measured as the arithmetic mean of 18 measurements. For fly ash from the dump it is  $9,1 \text{ Bq}\cdot\text{kg}^{-1}$  and is greater than for fly ash from an electro-filter ( $7,9 \text{ Bq}\cdot\text{kg}^{-1}$ ) and background activity ( $7,1 \text{ Bq}\cdot\text{kg}^{-1}$ ).

The  $\beta$ -activity of samples is due to isotopes of Potassium-40 and Rubidium-87 [1]. The content of isotope  $^{40}\text{K}$  in natural Potassium is  $\sim 0,01 \%$ .

The decrease in the amount of any radioactive material with the passage of time due to the spontaneous emission from the nuclei of either alpha or beta particles, often accompanied by gamma radiation. Gamma spectrum of the studied samples is shown on Figure 6.

On the spectra, the characteristic peaks of the isotopes of Lead, Bismuth, Cesium and Potassium manifested. It should be noted, that Cesium is a beta-

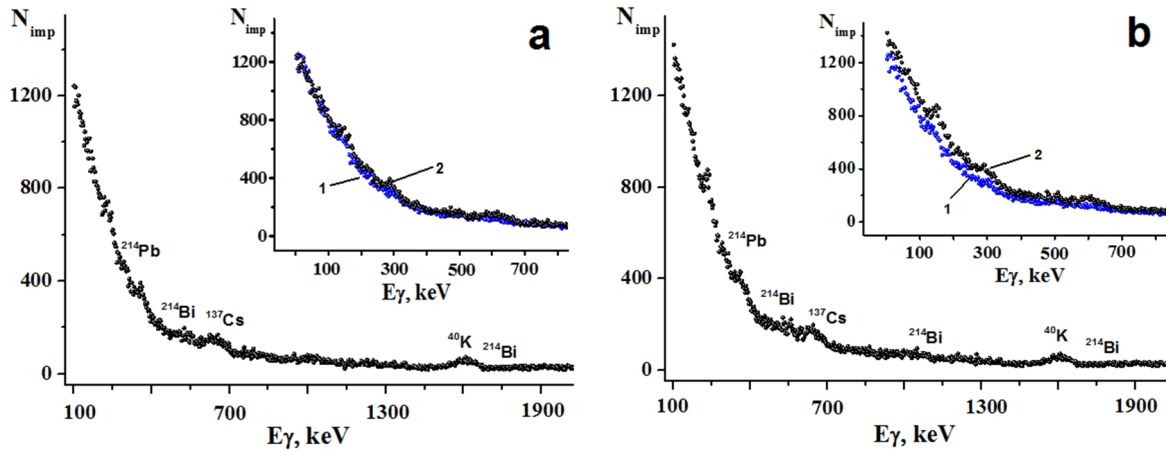


**Fig. 6.**  $\gamma$ -spectra of fly ash, selected from an electro-filter (a) and selected from a dump (b). On the insets: spectrum of  $\gamma$ -activity of fly ash from an electro-filter (a) and fly ash from the dump (b) in the energy range 100 to 700 keV, in comparing with background activity.

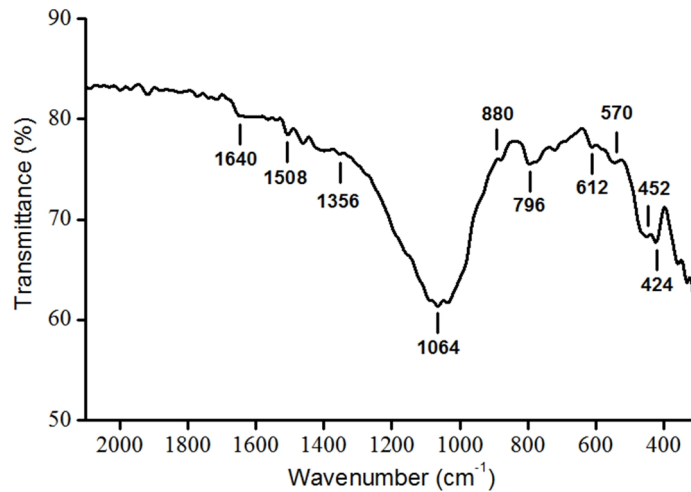


**Fig. 5.** FTIR spectrum of fly ash.

emitter, but the line of 661 keV gives its daughter isotope  $^{137m}\text{Ba}$  in metastable state ( $^{137m}\text{Ba}$ ).

The gamma spectrum of fly ash from an electro-filter in the energy range from 100 to 700 keV is close to the background spectrum. However, the gamma spectrum of fly ash from the dump in the energy range 100-700 keV indicates the higher gamma activity of this material.

This activity is due to the long storage of fly ash in the dump and mainly due to  $^{222}\text{Rn}$  decay products.  $^{222}\text{Rn}$ , formed in the Earth's bowels, results in  $^{226}\text{Ra}$  decay, percolates outward, contacts with particles of fly ash and adsorbs on their surface.

The half-life of  $^{222}\text{Rn}$  is only 3,1 minute. Adsorbed  $^{222}\text{Rn}$  is rapidly decay in to  $^{214}\text{Pb}$  ( $E_{\beta}=1000$  keV;  $E_{\gamma}=295$  keV, 352 keV);  $^{214}\text{Bi}$  ( $E_{\beta}=3200$  keV,  $E_{\gamma}=609, 1120, 1760$  keV) [20-22], which are transformed in to  $^{210}\text{Pb}$  and stable  $^{206}\text{Pb}$ .

The accumulation of these isotopes on the surface of fly ash particles leads to an increase its  $\beta$ - and  $\gamma$ -activity.

The common specific activity of fly ash from an electro-filter is  $200,4 \pm 39,6$  Bq $\cdot$ kg $^{-1}$ ; fly ash from the dump  $313,2 \pm 59,1$  Bq $\cdot$ kg $^{-1}$ . According to ref. [23], fly ash

from an electrofilter and fly ash from the dump with such specific activities have no restrictions on their practical use.

## Conclusions

1. Fly ash particles formed in a flame during coal combustion are crystallized glass spheres with a size of 0.8 – 600  $\mu\text{m}$ . The fly ash fraction with the size of 0.8 - 32 microns is dominates in the powder material and its volume is 54.8%.

2. Micro-spheric particles of fly ash are heterogeneous in chemical composition. In particular, the mass content of iron oxides in spheres varies from 2.1% to 96.4%. However, despite the different chemical composition, the mass ratio of  $\text{Al}_2\text{O}_3/\text{SiO}_2$  in fly ash particles is a constant  $0.47 \pm 0.02$ .

3. Phase analysis shows the presence of  $\alpha$ -quartz ( $\sim 62$  wt%) in micro-spherical particles,  $\text{Al}_{2,4}\text{Si}_{0,6}\text{O}_{4,8}$  mullite ( $\sim 32$  wt%), and mixtures of goethite, hematite and magnetite (total 6 wt%). In particles with high

content of ferrous oxides, the main phases are microcrystalline  $\alpha$ -quartz (~ 29 wt%), magnetite (~ 50 wt%) and hematite (~ 21 wt%).

4. An increase in the specific volume of microcrystallites formed inside the glass spheres causes considerable mechanical strain in the particles, which in turn leads to an increase in their hardness.

5. The higher  $\beta$ - and  $\gamma$ -activity of the fly ash from the dump compared to fly ash from the electro-filter is due to accumulation of the  $^{222}\text{Rn}$  decay products such as  $^{214}\text{Pb}$ ,  $^{214}\text{Bi}$ ,  $^{210}\text{Pb}$  on the surface of fly ash particles.

**Mironyuk I.F.** - Doctor of Chemical Science, Professor, Head of the Department of Chemistry;  
**Tatarchuk T.R.** - Ph.D., Assistant Professor, Department of Chemistry, Director of the Scientific and Research Center of Material Science and Nanotechnologies;  
**Vasylyeva G.V.** - Ph.D., Associate Professor of the Department of Theoretical Physics;  
**Yaremiy I.F.** - Doctor of Physical Science, Professor of the Department of Materials Science and Novel Technologies;  
**Mykityn I.M.** - Ph.D., Associate Professor of the Department of Chemistry.

- [1] V.V. Zyryanov, D.V. Zyryanov, Zola-unosa – tehnogennoe syire (NNTs «Maska», Moskva, 2009).
- [2] A.V. Stepanov, Dostizheniya energetiki i zaschita okruzhayushey sredy (Naukova dumka, Kiev, 2004).
- [3] N.S. Timoschuk, I.S. Bobyik, Primenenie zolyi i shlaka Burshtyinskoy GRES v zhelezobetonnyih izdeliyah dlya dorozhnoho stroitelstva (Mir, Moskva, 1991).
- [4] E.I. Putilin, V.S. Tsvetkov, Obzornaya informatsiya otechestvennogo i zarubezhnogo opyita primeneniya othodov ot tverdogo topliva na TES (SoyuzDorNII, Moskva, 2003).
- [5] Z.B. Entin, L.S. Nefedova, N.V. Strzhalkovskaya, Tsement i ego primenennye, 2, 40 (2012).
- [6] E.E. Berry, V.M. Molhotra, ACIJ, 2(3), 59 (1982).
- [7] Z.T. Yao, X.S. Ji, P.K. Sarker et al, Earth-Science Reviews, 141, 105 (2015).
- [8] A.G. Malchik, S.V. Litovkin, Mezhdunarodnyiy zhurnal prikladnyih i fundamentalnyih isledovaniy 9, 23(2005).
- [9] T.S. Rushad, A. Kumar, S.K. Dugga et al. International Journal of Civil and Structural Engineering 1(4) 2011.
- [10] P.Villars, K.Cenzual, R.Gladyshvskii, Handbook of Inorganic Substances. (Boston: De Gruyter, Berlin, 2014).
- [11] I.F.Mironyuk, V.L.Chelyadin, R.R.Yakubovskiy, V.O.Kotsyubinskiy, Fizika i himiya tverdogo tila, 11(2), 409 (2010).
- [12] T.Tatarchuk, M.Bououdina, Judith J.Vijaya, J. Kennedy. In: Fesenko O., Yatsenko L. (eds) Nanophysics, Nanomaterials, Interface Studies, and Applications. NANO 2016. Springer Proceedings in Physics, Springer, 195, 305 (2017), [https://doi.org/10.1007/978-3-319-56422-7\\_22](https://doi.org/10.1007/978-3-319-56422-7_22)
- [13] A.I.Efimov, L.P.Belorukova, I.V.Vasil'kova, V.P.Chechev, Svoystva neorganicheskikh soedinenij. Spravochnik. (Himiya, Leningrad, 1983).
- [14] W. Höland, G.H. Beall. Glass-Ceramic Technology. Second edition (American Ceramic Society, 2012).
- [15] A.P. Legrand, The Surface Properties of Silicas (Wiley, New York, 1998).
- [16] H. F. Chen, G. D. Wei, X. Han et al. Journal of Materials Science: Materials in Electronics 22, 252 (2011).
- [17] I.F. Myronyuk, V.I. Mandzyuk, V.M. Sachko, V.M. Gun'ko, Nanoscale Research Letters 11 (508), 1(2016).
- [18] L.YA. Kizil'shtejn, Himiya i zhizn', 2, 24(2006).
- [19] R.A. Zielinski. Radioactive Elements in Coal and Fly Ash: Abundance, Forms, and Environmental Significance (U.S. Geological Survey, 1997).
- [20] V.E. Guiseppe, S.R. Elliott, A. Hime, K. Rielage, S. Westerdale. AIP Conference Proceedings 1338, 95 (2011).
- [21] J. Argyriades, R. Arnold, C. Augier et al. Nuclear Instruments and Methods in Physics Research Section A: Accelerators, Spectrometers, Detectors and Associated Equipment, 606 (3), 449 (2009)
- [22] E. De la Cruz, R. Gonzalez et al. Rev. Int. Cont. Ambient 27(3), 2011.
- [23] Normi radiacijnoi bezpeki Ukraïni (NRBU-97) (Kiïv, 1997).

І.Ф. Миронюк<sup>1</sup>, Т.Р. Татарчук<sup>2</sup>, Г.В. Васильєва<sup>3</sup>, І.П. Яремій<sup>4</sup>, І.М. Микитин<sup>1</sup>

## Морфологія, фазовий склад та радіологічні властивості золи виносу Бурштинської теплової електростанції

<sup>1</sup>Кафедра хімії, ДВНЗ «Прикарпатський національний університет імені Василя Стефаника»,  
Івано-Франківськ, 76018, Україна, [myrif555@gmail.com](mailto:myrif555@gmail.com)

<sup>2</sup>Навчально-науковий центр хімічного матеріалознавства та нанотехнологій, ДВНЗ «Прикарпатський  
національний університет імені Василя Стефаника», Івано-Франківськ, 76018, Україна, [tatarchuk.tetyana@gmail.com](mailto:tatarchuk.tetyana@gmail.com)

<sup>3</sup>Відділення фізики ядра і елементарних частинок, кафедра теоретичної фізики, Ужгородський національний  
університет, 88000, Ужгород, Україна, [hanna.vasylyeva@uzhnu.edu.ua](mailto:hanna.vasylyeva@uzhnu.edu.ua)

<sup>4</sup>Кафедра матеріалознавства та новітніх технологій, ДВНЗ «Прикарпатський національний університет  
імені Василя Стефаника», Івано-Франківськ, 76018, Україна, [yaremiyip@gmail.com](mailto:yaremiyip@gmail.com)

Досліджено фізико-хімічні властивості золи, що вилучається з диму під час згорання вугілля на Бурштинській тепловій електростанції. Утворені в полум'ї частинки є закристалізованими скляними кульками з розміром 0,8 – 600 мкм. З'ясовано, що частинки золи неоднорідні за хімічним складом. Масовий вміст оксидів феруму в них може змінюватися в межах від 2,1 % до 96,4 %, однак, незважаючи на це, співвідношення  $Al_2O_3/SiO_2$  в кульках залишається величиною сталою, рівною  $0,47 \pm 0,02$ . Фазовий аналіз підтвердив наявність у частинках  $\alpha$ -кварцу (~ 62 мас. %), муліту (~ 32 мас. %) та суміші  $\alpha$ -FeOOH,  $\alpha$ -Fe<sub>2</sub>O<sub>3</sub> і Fe<sub>3</sub>O<sub>4</sub> (разом 6 мас. %). Радіологічні дослідження виявили вищу  $\beta$ - і  $\gamma$ -активність золи, відібраної з відвалу, порівняно із золою з електрофільтру. Це зумовлено накопиченням на поверхні вказаних частинок радіонуклідів <sup>214</sup>Pb і <sup>214</sup>Bi, які утворюються внаслідок розкладу адсорбованого <sup>222</sup>Rn.

**Key words:** зола виносу, скляні мікросфери, муліт, кварц, радіологія.